



LAWRENCE
LIVERMORE
NATIONAL
LABORATORY

The Application of Compressed Magnetic Fields to the Ignition and Thermonuclear Burn of Inertial Confinement Fusion Targets

L. J. Perkins, B. G. Logan, G. B. Zimmerman, C. J. Werner

March 20, 2013

Physics of Plasmas

Disclaimer

This document was prepared as an account of work sponsored by an agency of the United States government. Neither the United States government nor Lawrence Livermore National Security, LLC, nor any of their employees makes any warranty, expressed or implied, or assumes any legal liability or responsibility for the accuracy, completeness, or usefulness of any information, apparatus, product, or process disclosed, or represents that its use would not infringe privately owned rights. Reference herein to any specific commercial product, process, or service by trade name, trademark, manufacturer, or otherwise does not necessarily constitute or imply its endorsement, recommendation, or favoring by the United States government or Lawrence Livermore National Security, LLC. The views and opinions of authors expressed herein do not necessarily state or reflect those of the United States government or Lawrence Livermore National Security, LLC, and shall not be used for advertising or product endorsement purposes.

The Application of Compressed Magnetic Fields to the Ignition and Thermonuclear Burn of Inertial Confinement Fusion Targets

L. J. Perkins, B. G. Logan, G. B. Zimmerman, C. J. Werner
Lawrence Livermore National Laboratory, Livermore CA 94550, USA

We report for the first time on full 2-D radiation-hydrodynamic implosion simulations that demonstrate the impact of highly compressed magnetic fields on the ignition and burn of spherically-converging inertial confinement fusion targets with application to the National Ignition Facility indirect-drive ignition capsule. Initial seed fields of 20-100T (potentially attainable using present experimental methods) that compress to greater than 10^4 T (100 MG) under implosion can relax hotspot areal densities and pressures required for ignition and propagating burn by $\sim 50\%$ in targets degraded by lower-mode perturbations compared to those with no applied field. This accrues from range shortening and magnetic mirror trapping of fusion alpha particles, suppression of electron heat conduction and potential reduction of hydrodynamic instability growth. This may permit the recovery of ignition, or at least significant alpha particle heating, in submarginal capsules that would otherwise fail because of adverse low-mode hydrodynamic instabilities.

PACS numbers: 52.57.-z 28.52.Cx

In inertial confinement fusion (ICF), around a milligram of deuterium-tritium (DT) fusion fuel is rapidly compressed to high densities and temperatures sufficient for thermonuclear fusion to commence. Complete burning of a 50:50 mix of DT through the reaction ${}^2\text{H} + {}^3\text{H} \rightarrow \text{n} + {}^4\text{He} + 17.6\text{MeV}$, releases a specific energy of 3.38×10^{11} J/g. The National Ignition Facility (NIF) is seeking to demonstrate laser-driven ICF ignition and fusion energy gain in the laboratory for the first time by means of indirect-drive where laser energy is first converted to x-rays in a hohlraum surrounding the fuel capsule [1]. The absorbed radiation implodes the capsule until spherical convergence and gas backpressure decelerates the shell, compressing its solid fuel, and converting its kinetic energy into PdV work on a central gas “hotspot”. Under appropriate conditions, this can initiate fusion ignition, i.e., a thermonuclear deflagration burn wave propagating out from the hotspot into the compressed fuel via deposition of the 3.5 MeV alpha particles from the DT reaction.

The NIF ignition campaign has made significant progress with around thirty cryogenic-DT target implosions returning experimental data of unprecedented value [2,3]. The quality of implosions has progressed substantially but, at present, the fusion yield remains a factor of ~ 10 lower than required to initiate bootstrap alpha heating, and the fuel is compressing to around one-half that required for ignition [4,5]. The criteria for ignition and propagating burn are determined by the time-dependent balance between hotspot energy gains (shell PdV work and fusion alpha deposition) and losses (hydrodynamic expansion, electron heat conduction and radiation) [6]. Achievement of ignition in the

conventional situation of no applied magnetic field requires the attainment of a well-formed hotspot with central ion temperature of $T_i \sim 12$ keV, an areal density of $\rho R_h \sim 0.5$ g/cm² and pressure of around 10^{17} Pa (1000GBar) [7]. It is the purpose of this paper to demonstrate that the application of external axial magnetic fields that compress to high values under NIF implosion conditions may relax the hotspot conditions required for ignition and thermonuclear burn. In particular, such applied fields may recover ignition in submarginal capsules that would otherwise fail because of deleterious hydrodynamic instabilities.

When an ICF capsule is compressed in an applied magnetic field, the highly conducting plasma is characterized by large Magnetic Reynolds Numbers $R_m \gg 1$, the ratio of the magnetic advection to magnetic diffusion UL/η – where UL is a product of the velocity and length scales, η is the magnetic diffusivity that scales as $\sim \nu_{ei} \sim 1/T_e^{3/2}$, ν_{ei} is the electron-ion collision frequency and T_e is the electron temperature. NIF capsule implosion times are ~ 15 ns while magnetic resistive diffusion times are $\sim \mu$ s, thus the flux is effectively frozen in and the magnetic field compresses to high factors. The potential advantages of strong magnetic fields in ICF were recognized four decades ago [8,9], followed by a number of numerical studies [10,11,12,13] and recent concepts [14,15]. Magnetizing a plasma with compressed field B reduces electron heat conduction perpendicular to the field as $k_{\perp} \nabla T_e$ – where $k_{\perp} = k / (1 + (\omega_{ce} \tau_{ei})^2)$ and where k is the normal (zero field) thermal conductivity, ω_{ce} ($\sim B$) is the electron gyrofrequency in the magnetic field and τ_{ei} the electron-ion collision time [16] – requiring compressed fields around $\sim 10^3$ T (10 MG). Stronger compressed fields of $\sim 10^4$ T (100 MG) can localize the deposition range of charged fusion burn products within the hotspot to around that of their gyro orbit $(2mE)^{1/2}/qB$, which, for the 3.5 MeV DT alpha particle, is $\sim 54/B(\text{T})$ cm.

Fig.1 shows the NIF indirect drive ignition platform employed for these studies, where the DT fuel capsule is mounted in the center of a cylindrical gold hohlraum [2,3]. The hohlraum is illuminated with 192 laser beams with a total laser energy typically in the range 1.5-1.7 MJ to produce a soft x-ray flux with ~ 300 eV temperature. In the simulations for this paper, the applied axial seed magnetic fields are directed as shown along the cylindrical (z) axis of the hohlraum. Laser-driven magnetic flux compression within a cylindrical ICF target has been performed on the OMEGA laser facility, where a pair of small co-located Helmholtz coils generated a initial seed field of $\sim 16(9)$ T at the coil(target) and achieved a field compression factor of $\sim 10^3$ [17,18]. In recent laser-driven magnetized implosions in spherical geometry on OMEGA, a seed field of ~ 8 T was generated in a spherical target by a single coil with diameter around twice that of the capsule [19]. The compressed field attained central value of 8000 T (80 MG). As a result of the hot-spot magnetization, observed ion temperatures and neutron yields were enhanced by 15% and 30%, respectively, relative to non-magnetized controls. Very high seed fields are attainable with laser-driven coils due to their very low inductance and high current rise [20]. Recently, Fujioka et al. demonstrated laser-generated seed fields over 1000 T (10 MG) in a ~ 1 mm capacitor-coil system using 1 kJ, 1.3 ns, $0.1-4 \times 10^{16}$ W/cm² beams from the GEKKO-XII laser [21,22]. It is beyond the scope of this letter to examine engineering details for prospective NIF target coil systems. However, we note that the NIF hohlraum itself might serve as a single turn solenoid containing a narrow insulating gap parallel to the hohlraum axis and driven either by a co-located pulsed power supply

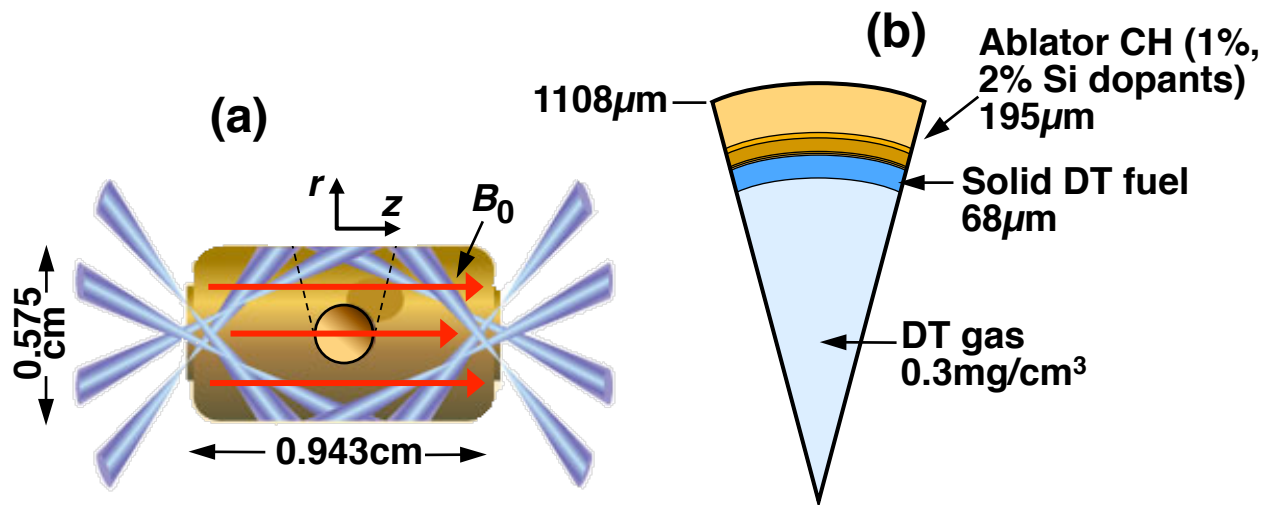


FIG. 1. (a) The NIF ignition target comprising cylindrical gold hohlraum and cryogenic DT fuel capsule (b) Fuel capsule radial build and composition used for this study

and transmission line for $B_0 \lesssim 20$ T or perhaps by one quad of NIF beams (~ 35 kJ) for $B_0 \lesssim 100$ T

Fig. 1b illustrates the NIF ignition capsule modeled in our simulations. It has a 68- μm -thick DT fuel layer and a 195- μm -thick doped-CH ablator, typical of the range of capsules used for the layered cryogenic implosion experiments to date [2,3]. The ablator consists of five plastic layers, three of which are doped with 1%, 2%, and 1% Si that absorb higher frequency non-Planckian preheat radiation, thereby tailoring the temperature and density profiles to minimize instability growth. Simulations in this paper were conducted in 2-D with the LASNEX radiation-hydrodynamics code [23]. We first performed a 2-D integrated hohlraum-capsule calculation to model relevant physics in the laser propagation, x-ray conversion and capsule absorption processes. (The impact of the initial applied seed magnetic fields on hohlraum plasma conditions and possible beneficial effects therein – e.g., potential suppression of hohlraum wall blow-off, Landau damping of stimulated Raman and Brillouin scattering, restricting the range of preheat electrons, etc. – were not included here but may be fruitful in future work). We then performed a number of 2-D capsule-only simulations under the applied seed magnetic fields (detailed below), where only the imploding capsule was modeled with the surrounding hohlraum replaced by an x-ray drive mapped from the frequency-dependent source from the integrated hohlraum calculation.

The present NIF capsule which has yet to achieve ignition may be constrained by hydrodynamic instabilities that result in detrimental hotspot perturbations and cold-fuel/gas mix [24]. Recent neutron imaging and spectroscopy indicate the presence of appreciable low-mode asymmetries in the cold compressed fuel [25] while simulations of the implosions suggest that large-amplitude shape asymmetries resulting from low order Rayleigh-Taylor (RT) growth may be causing spatial variations in capsule and fuel momentum that prevent the DT ice layer from being decelerated uniformly by the hot spot pressure [26]. In our simulations, standard initial “roughness” perturbations were applied at the seven capsule interfaces – namely the outer ablator surface, the four internal doped ablator interfaces, the fuel-ablator interface and the ice-gas interface (Fig. 1b) – and where the perturbation mode spectra are characteristic of measured layering tolerances [2]. For this study only lower mode perturbations up to mode numbers $l = 2\pi r/\lambda = 30$ were included. In the solid black line of Fig. 2, we show the 2-D fusion yield performance from our LASNEX simulations of this capsule with no applied magnetic field as a function of the multiplier f_{pert} on the amplitude of the outer ablator surface perturbation with all other perturbations maintained at their nominal X1 values. Such increasing outer surface perturbations can be taken to represent either greater than nominal surface roughness or approximate surrogates for, e.g., low mode perturbations in the radiation drive resulting from line-of-sight M-band ($\gtrsim 1.8$ keV) and N-band (~ 1 keV) emissions from the gold hohlraum, isolated modes such as the Mylar capsule support tent in the hohlraum (equivalent mode number of ~ 15), or other such asymmetric disturbances. In this way we are able to increase the lower mode perturbation until the capsule fails to ignite and then assess potentially ameliorating effects due to applied magnetic fields.

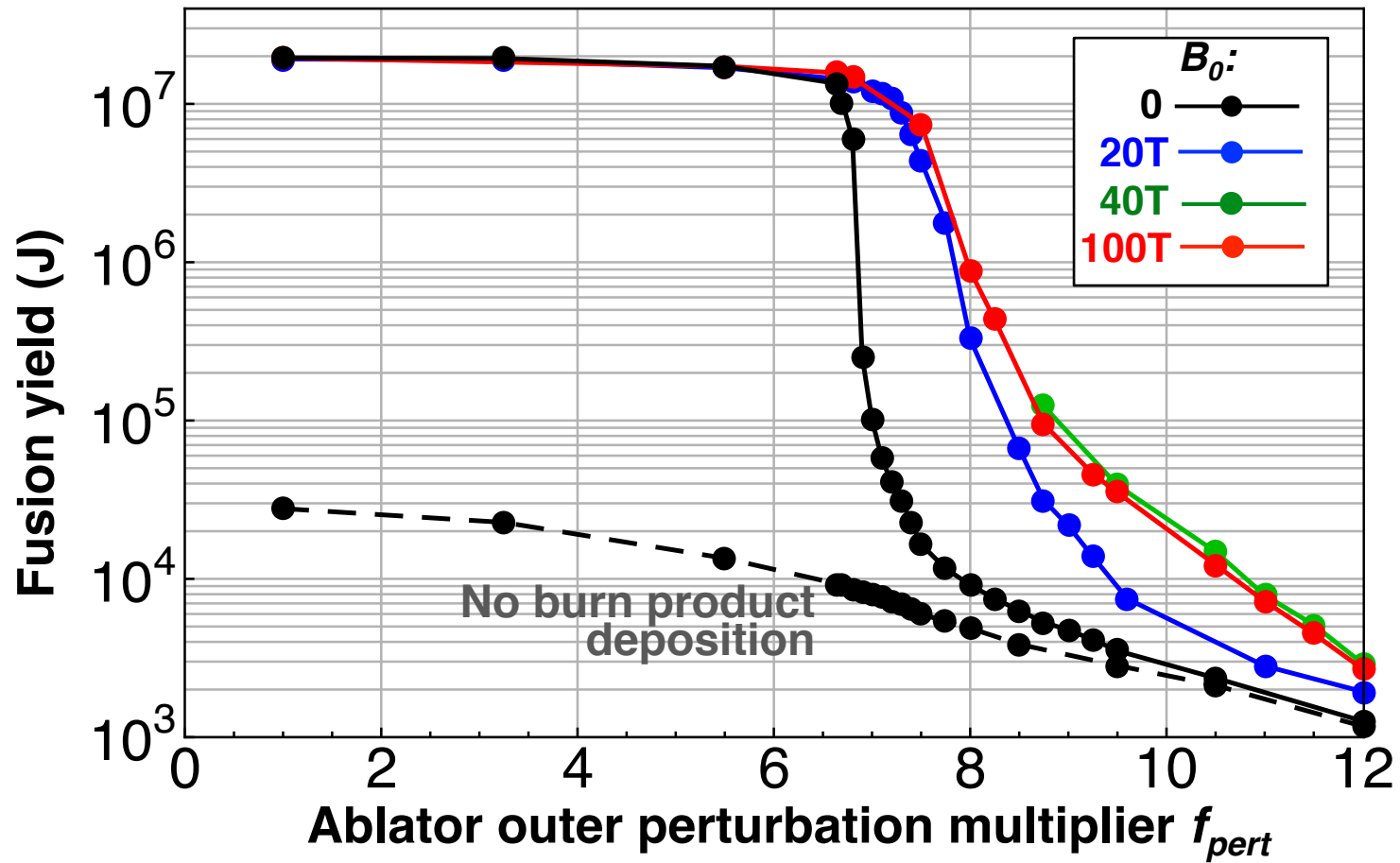


FIG. 2. Target fusion yield versus multiplier on the amplitude of capsule outer surface perturbation under initial seed magnetic fields from 0 to 100 T. The dashed line shows the fusion yield for $B_0 = 0$ with all fusion burn products allowed to escape without energy deposition

The solid black ignition curve in Fig. 2 is characterized by ignition and essentially full 19 MJ yield from $f_{pert} = 1$ to ~ 6.5 , an ignition “cliff” from $f_{pert} = \sim 6.5$ to 7.5 where fusion yield falls by three orders of magnitude, and a slowly decreasing, low yield region for $f_{pert} \gtrsim 7.5$. In the first of these, the capsule ignites at a central temperature of ~ 12 keV and peak values of the ion temperature during burn exceed 100 keV. In the latter low fusion yield region of the curve, the hotspot hydrodynamic parameters are determined only by the energy imparted by the perturbed stagnating shell and energy deposition from fusion alpha particles plays a negligible role. The dashed black line in Fig. 2 indicates the fusion yield performance of an identical capsule but allowing all fusion burn products (charged particle, neutrons and gammas) to escape the capsule with their full birth energy without deposition. Here, without bootstrap heating from deposited alpha particles, ignition is impossible at any value of f_{pert} and the fusion yield accrues only through modest hotspot heating (maximum $T_i \sim 5$ keV) from shell PdV work. Comparison of the two black curves indicates that fusion yields of around ~ 25 kJ (i.e., 5 kJ of deposited alpha energy) will likely be required for detection of alpha particle heating, while success in achieving ignition is taken to be a fusion yield of around 1 MJ. In the latter, the energy deposited by alphas (200 kJ) is around ten times that of the shell PdV work and thus dominates the subsequent hydrodynamic parameters. The ignition temperature of 12 keV is then obtained through bootstrap heating and peak ion temperatures here rise to ~ 40 keV resulting from the alpha-propagated burn wave.

In LASNEX, arbitrary 3-D magnetic field geometries can be imposed by user-specified sources. Here we specify an initial axial field B_0 , parallel to the hohlraum axis as shown in Figure 1a. The magnetic field package includes $J \times B$ forces and the full Braginskii cross-field transport model, with coefficients [27] extended to handle degenerate matter [28], and incorporates magnetic diffusion. The simulation results of this paper also include, for the first time, full orbit-following-deposition of fusion burn product charged particles (dominated by the 3.5 MeV DT alpha) in the presence of the magnetic field for spherically-converging burning capsules. This is accomplished through solving the Lorentz force equation and applying the spatial-stepping particle push method [29] modified to include effects of continuous slowing.

Results of applying an external axial magnetic field is shown in Figure 2 where the blue, green and red lines show the fusion yield curves versus outer surface perturbation f_{pert} for initial seed fields of 20, 40 and 100T, respectively. The major effect is seen to be a shift of the ignition cliff to the right in that the capsule can now attain ignition and appreciable yields at perturbation parameters that would otherwise result in only low yield, non-igniting capsules. Further, even at very high shell perturbations of $f_{pert} \gtrsim 9$, fusion yields with the field are around an order of magnitude higher, with hotspot conditions enhanced over those resulting from shell PdV heating alone and indicating detectable alpha heating. Note also that at the nominal applied perturbation $f_{pert} = 1$, the capsule attains the full fusion yield of ~ 19 MJ irrespective of the applied field. Two previous studies have indicated that compressed fields can restrict alpha burn propagation into surrounding fuel leading to only low gains [11,13]. However, the first of these assumed an axis-encircling toroidal flux with closed field lines, while the second modeled a 1-D axial field in an infinite cylinder. Thus, in both cases, fusion alpha transport was effectively inhibited in all orthogonal directions. In our case of spherical compression of an axial field, alpha

particles are only inhibited in the radial direction. We caution that the ignition curve in Fig. 2 serves to indicate the degradation of ignition performance through low mode instabilities and the potentially ameliorating effects of compressed magnetic fields. It does not necessarily explain the present experimental performance of the NIF capsule which may also require assessment of high mode perturbations or other contributing effects [24].

Fig. 3a and 3b show the density contours in the r - z plane at ignition (defined at the time of an on-axis ion temperature of 12 keV) for capsules with no magnetic field and $B_0=100$ T, respectively, for the nominal outer perturbation amplitude multiplier of $f_{pert}=1$. The inner and outer black lines show, respectively, the radial positions of the hotspot boundary (radius of the half-height of the density profile) and outer shell boundary (1/e point on the density profile). For the case in Fig 3b, where the initial 100 T seed field was applied parallel to the z -axis, we show, in red, the compressed magnetic field lines at stagnation/ignition plotted at radii of increasing equal increments of magnetic flux. For purely 2-D axial compression, the axial field in the hotspot would scale with radius or density as $B_z \sim B_0 r^2 \sim B_0 \rho^{2/3}$ implying, for the average hotspot radius, a compressed field of $\sim 8 \times 10^4$ T (800 MG) relative to the initial 100 T seed field in the gas. The actual average value of the compressed vector field $(B_z^2 + B_r^2)^{1/2}$ across the hotspot in Fig 3b is 8.54×10^4 T (854 MG), i.e., a compression factor approaching 10^3 .

Both capsules in Fig. 3 exhibit well formed stagnation hotspots at this time with $T_i(0)=12$ keV, and ignition is followed by subsequent burn waves into the surrounding fuel shell for full fusion yields. However, the hotspot and shell parameters under which this occurs are quite different. In particular, the hotspot areal density and thermal pressure for the $B_0 = 100$ T case are only $\rho R_h = 0.254$ g/cm² and 464 GBar, respectively, compared to 0.515 g/cm² and 1200 GBar for the zero-field case. And whereas the shell areal densities are comparable at $\rho R = 0.990$ and 1.04 g/cm², respectively, the average shell DT density at ignition for $B_0 = 100$ T is only 743 g/cm³ compared to 1050 g/cm³ for the zero-field case. An additional consequence is that the case with field ignites 50 ps earlier under the same in-flight drive conditions.

Comparison of the density contours in Fig. 3 show two other interesting features for the $B_0=100$ T case – a smoother hotspot boundary with lower density nonuniformities across the shell suggesting possible suppression of RT growth (see below) and an asymmetric implosion at stagnation/ignition. Because of the $1/r^2$ nature of the field compression, inflight shell dynamics during implosion are unaffected by the applied field up to peak velocity. Even at ignition, the magnetic stagnation pressure $B^2/(2\mu_0)$ is only around 10% of the thermal pressure on average. However the spherical ablatively-driven shell compression together with the low mode shell perturbation around 45° , causes a more 3-D-like field compression at the capsule waist with a strong radial component (maximum values of the vector fields in this region approach 1.5×10^5 T (1500 MG)), while the flux previously frozen into the gas and the shell in this region must bend under spherical compression. Scaling the latter as a simple cantilever displaced from its equilibrium condition against the tension in the field lines provides a rough energy requirement of \sim kilojoules which must accrue at the expense of the kinetic energy for shell compression. The corresponding density contour plots for the $B_0 = 20$ T and 40T cases at $f_{pert}=1$ show,

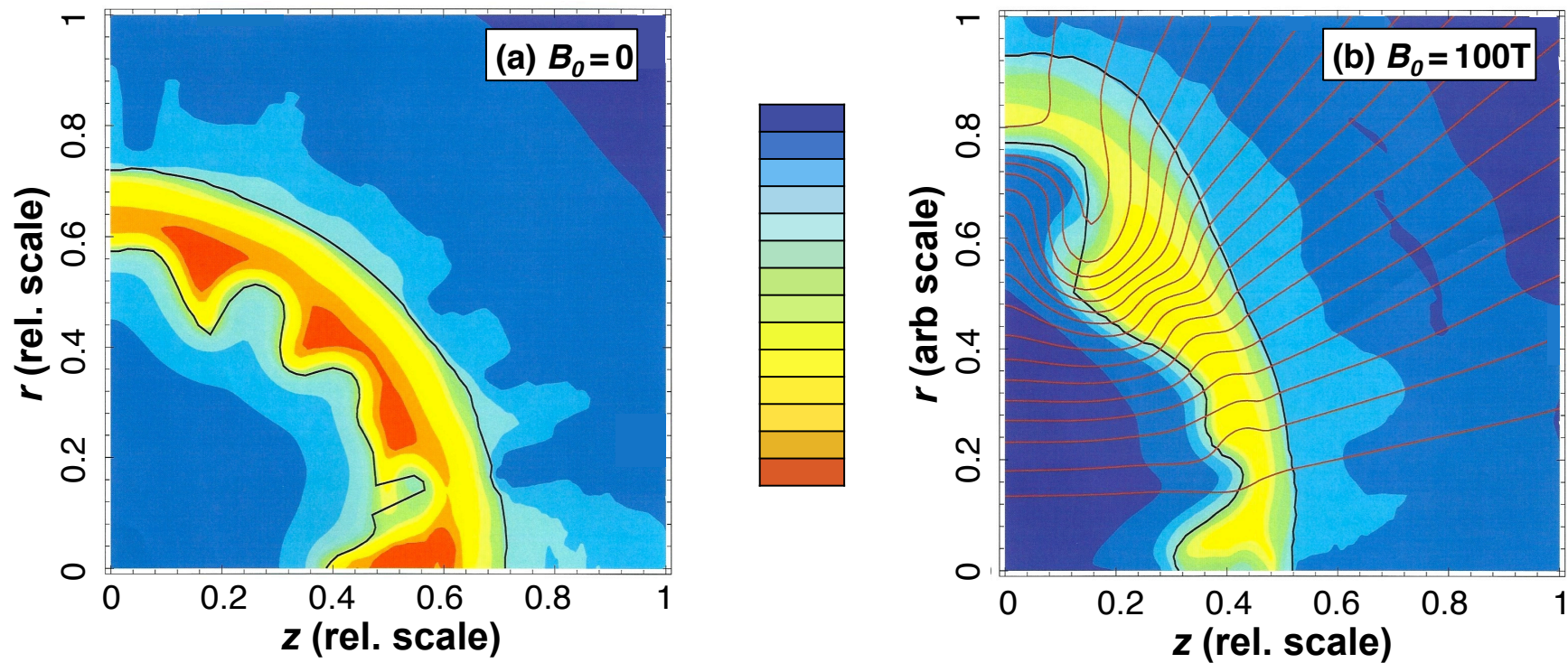


FIG. 3. Density contours at ignition for the nominal outer surface amplitude perturbation of X1 for initial seed magnetic fields of (a) zero, and (b) 100 T. The capsules are rotationally symmetric about the z -axis. Both targets attain a full, “clean-1D” fusion yield of 19.4 MJ.

respectively, no deviation and small-negligible deviation from sphericity at stagnation. The ignition conditions for the $B_0=40$ T case (green curve in Fig. 2) at $f_{pert}=1$ and $T_i(0)=12$ keV are $\rho R_h=0.247$ g/cm², $P_h=370$ GBar, and $\rho_{shell}=665$ g/cm³, comparable to those for the $B_0=100$ T case. Given this case also exhibits around the same fusion yield curve versus f_{pert} as $B_0=100$ T (Fig. 2) but requires a lower initial field suggests that around 40 T may be around the optimum seed field because it still maintains an essentially spherical hotspot at stagnation. This finding is contingent on only lower-mode perturbations up to $l=30$ and the optimum field may change in future work when we also consider high modes.

Fig. 4a and 4b show the corresponding density contours at stagnation for the high outer surface perturbation amplitude multiplier of $f_{pert}=8$ for capsules with no magnetic field and $B_0=100$ T, respectively, while Fig. 4c and 4d show the associated ion temperature contours. Here, there is a marked difference in fusion yield performance. The zero-field case obtains a fusion yield of only 9.1 kJ and a peak ion temperature of only 5 keV. Given this zero-field case does not ignite, the contours in Fig. 4a and 4c are plotted at time of the maximum value of $\int(\rho r T_i)_{HS}$ integrated over the hotspot. The contour plots for the case with field in Fig. 4b and 4d are plotted at ignition ($T_i(0)=12$ keV); this capsule attains a fusion yield of 0.89MJ – two orders of magnitude higher – and a peak ion temperature during burn of 36 keV. The magnetization parameter $\omega_{ce}\tau_{ei}$ varies from ~ 5 to 15 over the hotspot, thus perpendicular electron heat transport is fully suppressed; parallel transport is also reduced due to flux tube mirroring (see below). The average value of the compressed field across the hotspot is 9.15×10^4 T indicating 3.5MeV alpha deposition ranges perpendicular to B of the order of a gyro orbit of $\sim 54/B(\text{T}) = 6\mu\text{m}$, i.e., around one fifth of the hotspot radius. Thus, as above, ignition and burn is again achieved here with modest parameters of $\rho R_h=0.224$ g/cm², $P_h=538$ GBar, and $\rho_{shell}=431$ g/cm³

Gross shell perturbations due to hydrodynamic instabilities are evident in both cases in Fig 4a and 4b, but the case with field exhibits a more integral, compact shell with more uniform density, and a less perturbed hotspot boundary. Thus, as also evident when comparing Fig. 3a and 3b above, this is suggestive of lower growth of RT spikes during deceleration. The consequence of very high local values of $R_m > 10^4$ is that the magnetic flux must be locally conserved within developing spikes. Given the pressure gradient is opposite to the field gradient, then for the deceleration RT modes to grow they must locally forced sharp curvature of entrained flux that would increase field line bending energy and which, therefore, is stabilizing to interchange-like modes [30]. The bending energy for a flux tube scales as the square of the inverse radius of curvature, while the differential hydrodynamic pressure is linear with wavelength of the perturbation, thus we might expect increased stabilization for high modes. There is still a significant P4-like shell perturbation evident in the case with magnetic field in Fig. 4b that bends the upper portion of the flux passing through the hot spot into a noticeable magnetic mirror. Here, because magnetic moment is an adiabatic invariant, fusion alpha particles emitted with source angles greater than the mirror loss cone angle $\sin^{-1}(1/M) \sim 30^\circ$, where M is the mirror ratio $B(z)/B(0) \sim 4$ [30], will be mirror trapped within the hotspot. Given we track these orbits, such behavior is accommodated in the simulations. In principle, thermal electrons also experience mirroring but relax to an isotropic distribution due to their high collisionality; in any event, being thermal fluid particles, we do not track electron orbits

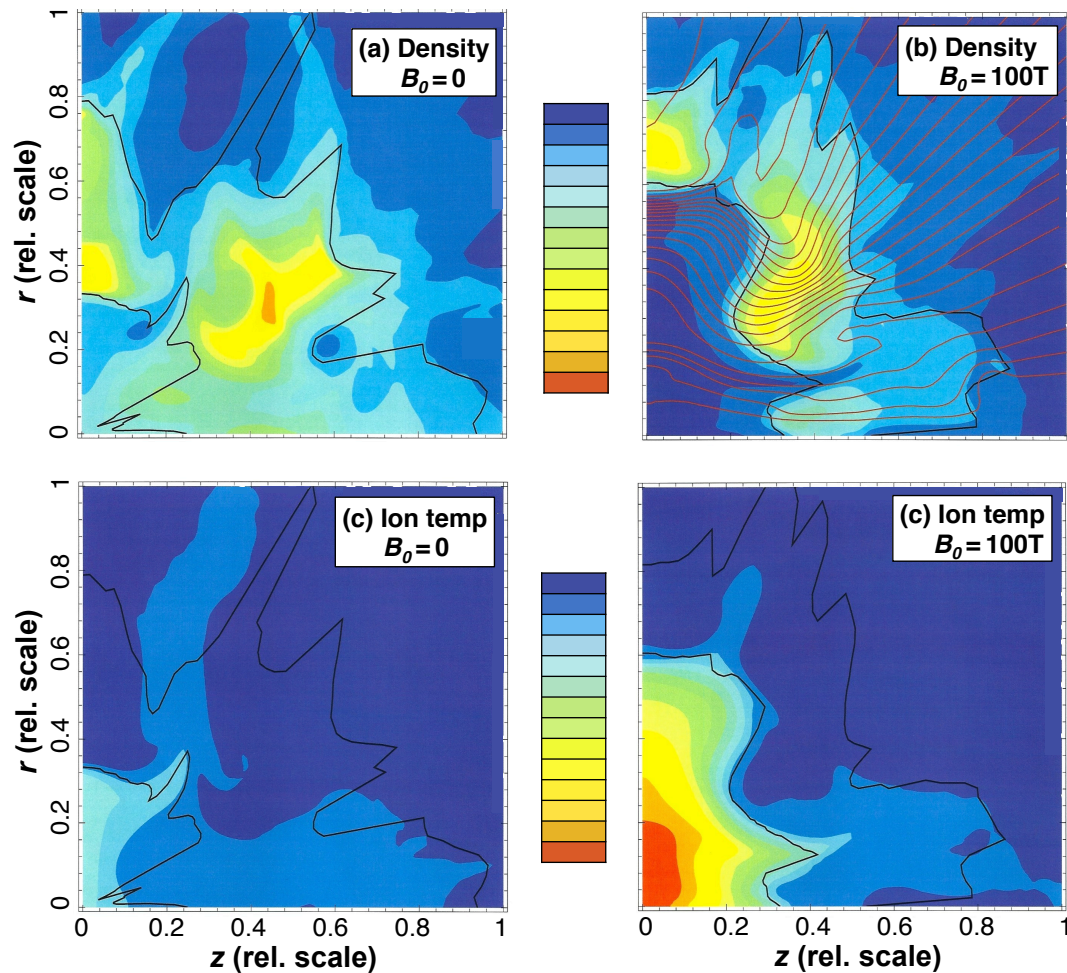


FIG. 4. Contours of density ((a), (b)) and ion temperature ((c), (d)) at stagnation for for initial seed magnetic fields of zero and 100 T, respectively, for a large outer surface amplitude perturbation of X8. Contours for the igniting 100T case (0.89 MJ fusion yield) are plotted at ignition, while those for the non-igniting zero-field case (0.0091 MJ fusion yield) are plotted at time of maximum $\int(\rho r T_\nu)_{HS}$.

in the magnetic field as we do for burn product charged particles. However, the high $\omega_{ce}\tau_{ei}$ will force electron heat conduction to follow the flux tube area and since the parallel conductivity is independent of density, the conduction loss is reduced by the area of the flux tube at the cold boundary where the peak flux occurs and is an additional factor reducing thermal heat loss. We note that it is feasible to consider engineering a 2-D, low mode ($\sim P2$) shim into the initial capsule shape to optimize the resulting mirror field under compression.

In conclusion, we have presented for the first time full radiation-hydrodynamic simulations indicating the recovery of ignition and propagating burn through the application of highly compressed magnetic fields in indirect-drive ICF targets degraded by low mode instabilities. We caution that the present results are contingent on a 2-D interpretation of the physical processes and only for lower mode outer surface perturbations up to $l = 30$. In addition, our 2-D simulations with their inherent azimuthal symmetry may overestimate the stabilizing effect of field line bending energy. Accordingly, future work will include: (1) 3-D simulations; (2) inclusion of characteristic high mode perturbations; (3) assessment of the impact of applied fields on hohlraum plasma conditions and potential benefits therein; (4) engineering P2 and P4 shims on the initial capsule thickness to augment compressed mirror ratios, and (5) optimization of capsule designs and drive conditions under an applied field – in particular, to achieve ignition at lower convergence ratios and the attainment of volumetric ignition in high-pressure non-cryogenic gas targets

We are pleased to acknowledge informative discussions with J. H. Hammer, J. H. Nuckolls, R. C. Kirkpatrick, D. D. Ho and W. E. Alley. This work was performed under auspices of U.S. DOE by Lawrence Livermore National Laboratory under Contract DE-AC52-07NA27344

-
- 1 J. D. Lindl *et al.*, Phys. Plasmas **11**, 339 (2004)
 - 2 S. W. Haan *et al.*, Phys. Plasmas **18**, 051001 (2011)
 - 3 S. H. Glenzer *et al.*, Phys. Plasmas **18**, 056318 (2012)
 - 4 O. Landen *et al.*, Plasma Phys Controlled Fusion **54** 124026 (2012)
 - 5 National Nuclear Security Administration, *Path Forward to Achieving Ignition in the Inertial Confinement Fusion Program* (U.S. Department of Energy, December 2012)
 - 6 R. Betti *et al.*, Phys. Plasmas **9**, 2277 (2002)
 - 7 J. D. Lindl, *Inertial Confinement Fusion* (AIP Press, Springer-Verlag, 1998)
 - 8 J. N. Olsen, *et al.*, J. Appl. Phys. **50**, 3224 (1979),
 - 9 I. R. Lindemuth and M. M. Widner, Phys. Fluids **24**, 753 (1981)
 - 10 M. A. Sweeney and A. Farnsworth, Nucl. Fusion **21**, 41 (1981)
 - 11 I. R. Lindemuth and R. C. Kirkpatrick, Nucl. Fusion **23**, 263 (1983)
 - 12 R. D. Jones and W. C. Mead, Nucl. Fusion **26**, 127 (1986)
 - 13 R. C. Kirkpatrick, I. R. Lindemuth, and M. S. Ward, Fusion Technology **27**, 201 (1995)
 - 14 S. A. Slutz *et al.*, Phys. Plasmas **17**, 056303 (2010)

-
- 15 S. A. Slutz *et al.*, Phys. Rev. Lett. **108** 025003 (2012)
 - 16 S. I. Braginskii, in *Reviews of Plasma Physics*, Vol. I, M. A. Leontovich(ed.) (Consultants Bureau, New York, 1965)
 - 17 O. V. Gotchev *et al.*, Phys. Rev. Lett. **103**, 215004 (2009)
 - 18 J. P. Knauer, *et al.*, Phys. Plasmas **17** 056318 (2010)
 - 19 P. Y. Chang, *et al.*, Phys. Rev. Lett. **107** 035106 (2011)
 - 20 H. Daido, *et al.*, Phys. Rev. Lett. **56** 846 (1986)
 - 21 S. Fujioka, *et al.*, Plasma Phys. Controlled Fusion **54** 124042 (2012)
 - 22 S. Fujioka, *et al.*, Sci. Rep. **3**, 1170; DOI:10.1038/srep01170 (2013)
 - 23 J. A. Harte, *et al.*, *LASNEX-A 2-D Physics Code for Modeling ICF*, UCRL-LR-105821-96-4, Lawrence Livermore National Laboratory (1996)
 - 24 D. S. Clark *et al.*, *Detailed Modeling of Deuterium-Tritium Layered Experiments on the National Ignition Facility*, Phys. Plasmas (to be published May 2013)
 - 25 G. Grim *et al.*, *Nuclear Imaging of the Fuel Assembly in Ignition Experiments*, Phys. Plasmas (to be published May 2013)
 - 26 R. H. H. Scott, *et al.*, Phys. Rev. Lett. **110** 075001 (2013)
 - 27 E. M. Epperlein and M. G. Haines, Phys. Fluids **29**, 1029 (1986).
 - 28 Y. T. Lee and R. M. More, Phys. Fluids **27**, 1273 (1984)
 - 29 J. P. Boris, in *Proc. 4th Conf. Numerical Simulations of Plasmas*, pp. 3-67, (Naval Res. Lab., Wash. D.C., 1970)
 - 30 T. Dolan, *Fusion Research* (Pergamon Press 1982, 2000)